IJIRCCE

ISSN(O): 2320-9801

ISSN(P): 2320-9798

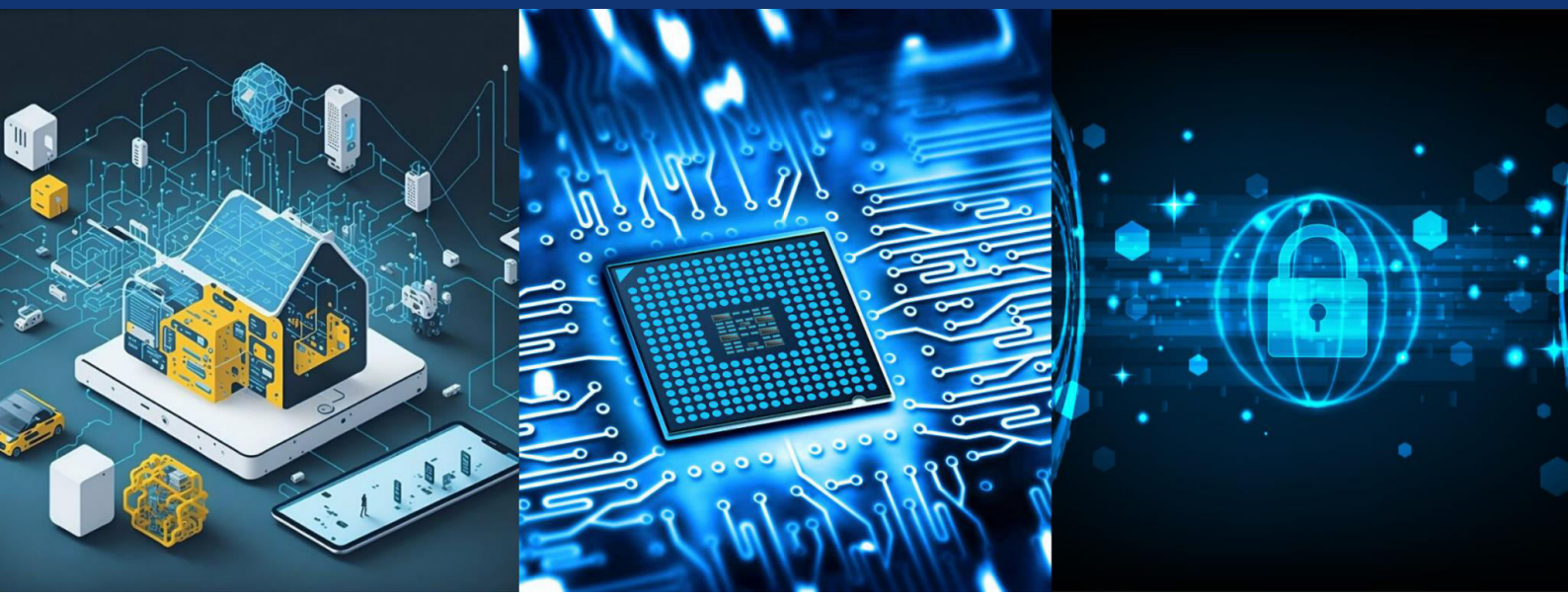

International Journal of Innovative Research in Computer and Communication Engineering

(A Monthly, Peer Reviewed, Refereed, Scholarly Indexed, Open Access Journal)

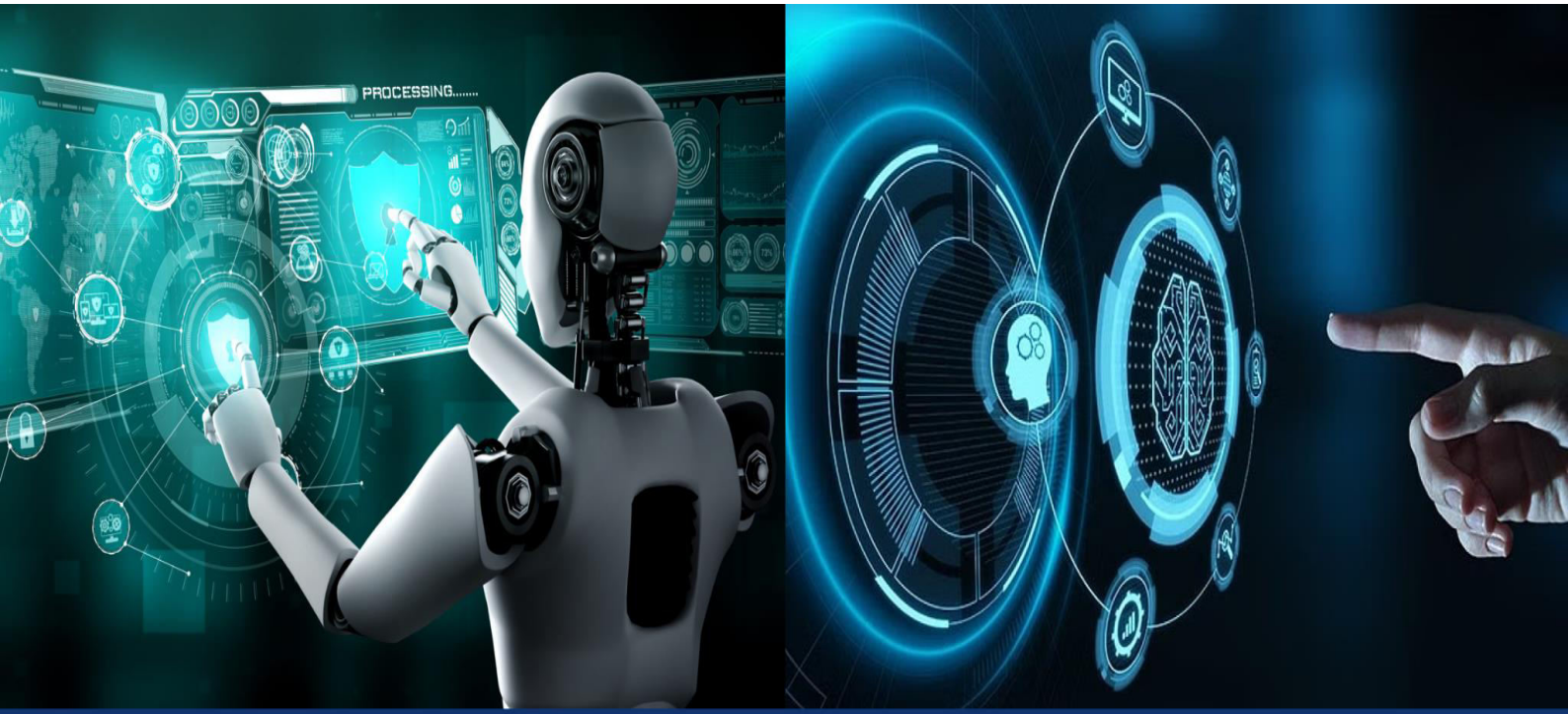

Impact Factor: 8.771

Volume 13, Issue 3, March 2025

© 2025 IJIRCCE | Volume 13, Issue 3, March 2025| DOI: 10.15680/IJIRCCE.2025.1303147

www.ijircce.com | e-ISSN: 2320-9801, p-ISSN: 2320-9798| Impact Factor: 8.771| ESTD Year: 2013|

International Journal of Innovative Research in Computer and Communication Engineering (IJIRCCE)

(A Monthly, Peer Reviewed, Refereed, Scholarly Indexed, Open Access Journal)

Digital Twin Implementation for Solar Cell Process Lines: Real-Time Simulation of PECVD, Diffusion, and Metallization for Predictive Process Control

Sekhar Tatineni

Vice President, Technology, Greenwood, South Carolina, USA

ABSTRACT: Solar cell manufacturing is a continuous process flow with strong cell-to-cell coupling through shared equipment, shared consumables, and overlapping recipe boundaries. A perturbation introduced anywhere in the flow propagates downstream and surfaces in final electrical characterization with delay determined by production cadence. Digital twin technology reverses the temporal direction of the engineering loop - shifting from retrospective detection to predictive control - and delivers compounding second-order benefits across energy efficiency, recipe throughput, and anomaly sensitivity. This article presents the theoretical architecture, modeling methodology, and control framework for a production-grade digital twin spanning PECVD, diffusion, and screen-print metallization processes in a PERC cell manufacturing environment. The architecture is organized into four functionally decoupled layers: Physical, Data, Twin, and Application, communicating through a bidirectional closed-loop channel. The twin layer employs a hybrid modeling stack that fuses first-principles physics models with data-driven machine learning surrogates, calibrated continuously against per-wafer production measurements using Bayesian posterior update methods. The predictive control engine achieves end-to-end control loop latency below 540 milliseconds and a predictive horizon of 90 minutes ahead of measurement-driven detection. The Bayesian recipe optimization engine evaluates 340 candidate recipes per minute by querying the twin rather than the physical line, representing an orders-of-magnitude improvement in process optimization throughput.

4-Layer	< 540 ms	90 min	340 / min
Twin Architecture	Control Loop Latency	Predictive Horizon	Bayesian Recipe Eval.

KEYWORDS: Digital Twin · Predictive Process Control · PERC Solar Cell Manufacturing · PECVD · Diffusion · Screen-Printing Metallization · Real-Time Simulation · Bayesian Optimization · Surrogate Modeling · Anomaly Detection · U.S. Domestic Manufacturing

I. WHY DIGITAL TWINS BELONG IN SOLAR CELL MANUFACTURING

1.1 The Engineering Challenge of Continuous Process Flow

Solar cell manufacturing is, at its core, a continuous process flow with strong cell-to-cell coupling through shared equipment, shared consumables, and overlapping recipe boundaries. A perturbation introduced anywhere in the flow propagates downstream and shows up in the final electrical characterization with a delay determined by the production cadence. The traditional engineering response to this propagation pattern has been retrospective: detect the disturbance after it has reached the final measurement, trace it back to its origin, and apply a corrective action that, by definition, cannot recover the cells already affected.

The manufacturing process for a PERC (Passivated Emitter and Rear Cell) solar cell involves approximately twelve sequential unit operations, from initial saw-damage removal and surface texturing through phosphorus diffusion, silicon nitride deposition, laser contact opening, screen-print metallization, firing, and final flash testing. Each step introduces process variability that interacts with the variability from previous steps in a multiplicative fashion. A diffusion furnace that drifts slightly toward higher temperatures will produce wafers with lower sheet resistance; those wafers, when

© 2025 IJIRCCE | Volume 13, Issue 3, March 2025| DOI: 10.15680/IJIRCCE.2025.1303147

www.ijircce.com | e-ISSN: 2320-9801, p-ISSN: 2320-9798| Impact Factor: 8.771| ESTD Year: 2013|

International Journal of Innovative Research in Computer and Communication Engineering (IJIRCCE)

(A Monthly, Peer Reviewed, Refereed, Scholarly Indexed, Open Access Journal)

subsequently processed through the PECVD step, may exhibit different surface chemistry interactions that subtly alter the passivation quality; and the combined effect of both variations may not be detectable until the final efficiency measurement - by which point several hours of production, representing tens of thousands of wafers, has already been committed.

This temporal gap between cause and effect is the defining challenge of continuous-process manufacturing control. It is also precisely the gap that digital twin technology is designed to close. A digital twin in a manufacturing context is a software construct that mirrors a physical production system continuously and bidirectionally. It ingests live sensor and process data, runs predictive models that simulate near-future system behavior, and emits control signals that close the loop back to the physical system.

The shift from retrospective to predictive engineering is the central operational benefit of digital twin deployment. Its second-order benefits - energy efficiency, recipe-search throughput, anomaly detection sensitivity - derive from the same mathematical infrastructure but address different commercial axes.

1.2 Theoretical Basis for Predictive Process Control

The theoretical basis for predictive process control via digital twin rests on three mathematical pillars. The first is the existence of a reliable forward model - a function that maps current process state and recipe parameters to predict future process outcomes with sufficient accuracy to be actionable. The second is the availability of real-time state estimation - the ability to determine, from available sensor measurements, the current state of the process in terms relevant to the forward model. The third is the existence of a controllable input space - process parameters that can be adjusted in real time with latency shorter than the time scale over which the process evolves toward undesirable states.

All three conditions are satisfied for the three process steps targeted in this article. Diffusion, PECVD, and metallization all have well-established physics-based models refined over decades of process science research. All three steps are instrumented with dense real-time sensor networks capable of providing sub-second state observations. And all three steps have continuously adjustable inputs - gas flow rates, temperatures, dwell times, pressures, squeegee parameters - that admit fine-grained adjustment by a control system operating at sub-second cycle times.

When these three conditions are met, the predictive control problem reduces to the following: at each time step t, given the current state estimate x(t) from sensors and the forward model f, compute the control input u*(t) that minimizes the expected future deviation from specification across all wafers currently in the process flow. Formally:

$$u^*(t) = \text{argmin}_u \; E[\, L(f(x(t), u), y\_spec) \,]$$

where L is a loss function measuring deviation from specification y_spec, and the expectation is taken over the uncertainty in the state estimate and model predictions. The digital twin architecture implements this optimization in real time, with the twin layer computing f and the application layer solving the optimization problem at every control cycle.

1.3 Why PECVD, Diffusion, and Metallization

Three process steps are prioritised for first-phase digital twin coverage on the basis of three criteria. First, each of the three is a high-leverage process step in the sense that small variations in its output materially affect final cell efficiency. Second, each is well represented by physics-based models that have been refined over decades of process science research and can be calibrated against production data. Third, each has continuous-time controllable inputs that admit fine-grained adjustment by a digital twin control output, in contrast to discrete-state steps where adjustment latency would compromise twin response.

Process Step	Primary Output	Efficiency Lever	Target Accuracy
Diffusion	Sheet resistance (Ω/□)	Voc, Fill Factor, Jsc	< 0.5 Ω/□ RMSE
PECVD	SiN_x thickness, n-index	Reflectance, recomb. vel.	< 0.5 nm RMSE
Metallization	Linewidth, contact resistance	Shadow loss, series R	< 0.5 µm RMSE

© 2025 IJIRCCE | Volume 13, Issue 3, March 2025| DOI: 10.15680/IJIRCCE.2025.1303147

www.ijircce.com | e-ISSN: 2320-9801, p-ISSN: 2320-9798| Impact Factor: 8.771| ESTD Year: 2013|

International Journal of Innovative Research in Computer and Communication Engineering (IJIRCCE)

(A Monthly, Peer Reviewed, Refereed, Scholarly Indexed, Open Access Journal)

Beyond these three primary steps, the digital twin architecture is designed to accommodate additional process steps in subsequent deployment phases. Edge isolation, firing, and final flash test are candidates for near-term expansion, each of which has physics-based model foundations documented in the semiconductor and photovoltaic processing literature.

1.4 Historical Context and Prior Art

Digital twin technology has its conceptual roots in the product lifecycle management (PLM) work of Michael Grieves at the University of Michigan in the early 2000s, formalized in the manufacturing context through the NASA Integrated Vehicle Health Management program around 2010. Production-grade implementations at scale have, until recently, been confined largely to discrete-part assembly industries - automotive and aerospace - where the relatively long cycle times and high per-unit value justify extensive per-unit modeling investment.

The application of digital twin technology to continuous-process semiconductor and solar manufacturing presents distinct challenges not present in discrete-part assembly. The per-wafer value is lower, requiring the twin's computational cost to be amortized across the full production volume. The process cadence is higher - tens of thousands of wafers per day - requiring the twin's inference to operate at sub-second cycle times. And the process physics is more complex, involving coupled partial differential equations for diffusion, plasma chemistry for PECVD, and non-Newtonian fluid dynamics for metallization, each requiring specialized numerical methods and calibration strategies.

Recent advances in surrogate modeling - the construction of fast, data-driven approximations to expensive physics simulations - have made it possible to deploy these models at production cadence for the first time. The hybrid architecture described in this article, which combines physics-based models with machine learning surrogates, represents the current state of the art in continuous-process digital twin deployment.

II. TWIN ARCHITECTURE AND HYBRID MODELING STACK

2.1 Four-Layer Architecture

The digital twin architecture deployed in a production PERC cell environment is organized into four functionally distinct layers. The layered design is deliberate: it confines change to the layer where the change originates and prevents proliferation of dependencies across layer boundaries. This architectural principle - sometimes called the separation of concerns - is borrowed from enterprise software engineering and applied here to the physical-digital integration challenge.

Layer	Components	Primary Responsibility
L1 - Physical	Production equipment, in-situ sensors, PLCs, inline metrology stations, actuators	Source of live data; destination of control signals
L2 - Data	OPC-UA connectivity, time-series databases, MES integrations, Kafka streams, historian	Capture, normalize, persist sub-second sensor data; 99.97% delivery SLA
L3 - Twin	Physics models, ML surrogates, calibration engine, Bayesian optimizer, state projector	Predict future process state; maintain model-reality alignment
L4 - Application	Predictive control engine, recipe optimizer, anomaly detector, operations dashboard, MES dispatcher	Translate twin predictions into operational actions and recipe adjustments

The unidirectional data flow convention - sensor data flowing upward through the layers, control signals flowing downward - is enforced as an architectural invariant. No layer communicates directly with a non-adjacent layer; all inter-layer communication passes through the defined interfaces. This constraint simplifies debugging, facilitates independent layer scaling, and ensures that the insertion of additional process steps into the twin coverage can be accomplished without architectural modification.

2.2 Hybrid Modeling Approach - Physics and Surrogate

The twin layer is a hybrid modeling stack that combines first-principles physics models with data-driven machine learning surrogates. Each of the three covered process steps has both a physics model and an ML surrogate. The two coexist

© 2025 IJIRCCE | Volume 13, Issue 3, March 2025| DOI: 10.15680/IJIRCCE.2025.1303147

www.ijircce.com | e-ISSN: 2320-9801, p-ISSN: 2320-9798| Impact Factor: 8.771| ESTD Year: 2013|

International Journal of Innovative Research in Computer and Communication Engineering (IJIRCCE)

(A Monthly, Peer Reviewed, Refereed, Scholarly Indexed, Open Access Journal)

because they serve complementary purposes: the physics model provides the structural envelope within which the surrogate operates, and the surrogate provides the speed required for real-time inference at production cadence.

The physics models encode the conservation laws, thermodynamic equilibria, kinetic rate equations, and transport phenomena that govern each process step. They are parameterized by a set of calibration parameters that must be fitted to production data but whose physical interpretation is well understood. The models produce predictions that are, in principle, extrapolatable beyond the training data distribution - a property critical for evaluating novel recipes that have not yet been run in production.

The ML surrogates are trained on the output of the physics models combined with direct production measurements. They learn to emulate the input-output mapping of the physics model within the observed operating region at much lower computational cost. The surrogates are retrained on a rolling basis as new production data accumulates, ensuring that they remain calibrated to the current state of the equipment and consumables.

Process Step	Physics Model	ML Surrogate	Latency	Roll. Window
Diffusion	Fick's 2nd Law + $POCl_3$ rxn-diffusion	XGBoost ensemble (240 trees)	54 ms	5,000 wafers
PECVD	Continuum plasma + Langmuir-Hinshelwood	Random Forest (360 trees)	38 ms	5,000 wafers
Metallization	Non-Newtonian rheology + viscoelastic mesh	MLP Neural Network (4 layers)	76 ms	5,000 wafers
Firing	Heat transfer + Bi-Sn reflow kinetics	XGBoost regression ensemble	42 ms	5,000 wafers
Edge Isolation	Laser-material interaction analytical	Convolutional NN on EL signature	120 ms	3,000 wafers
Flash Test	Diode equation + lumped resistance	Empirical ridge regression	28 ms	8,000 wafers

2.3 Calibration Engine - Theory and Implementation

The calibration engine is the component of the twin that maintains alignment between model predictions and production reality. Without continuous calibration, even a well-designed physics model will drift out of alignment with physical reality as equipment ages, consumables are depleted, and operating conditions shift. The calibration engine addresses this challenge through a combination of statistical drift detection and Bayesian parameter estimation.

The theoretical foundation of the calibration engine is the state-space model:

$$y(t) = h(f(x(t), \theta(t))) + \varepsilon(t)$$

where $y(t)$ is the measured process output, f is the physics model parameterized by $\theta(t)$, h is the measurement function, and $\varepsilon(t)$ is measurement noise. The calibration engine estimates the time-varying parameter vector $\theta(t)$ from the history of production measurements.

Drift detection is implemented using the CUSUM (cumulative sum) algorithm applied to the model residuals. For each process parameter, the CUSUM statistic accumulates evidence of systematic deviation from the expected residual distribution. The algorithm is configured with a reference value of 0.5σ (half the residual standard deviation) and a decision threshold of 5σ (five times the standard deviation), providing a balance between sensitivity to genuine drift events and robustness against false alarms driven by measurement noise.

$$S(t) = \max(0, S(t-1) + (r(t) - k)) \quad \text{where } k = 0.5\sigma, \text{ alarm if } S(t) > 5\sigma$$

When the CUSUM algorithm signals a drift event, the calibration engine initiates a Bayesian posterior update. The prior distribution over the parameter vector θ is updated using the likelihood of the observed production data given the physics

model. For the calibration parameters that admit conjugate priors - activation energies, rate constants, and similar scalar parameters - the posterior update is computed in closed form. For parameters without conjugate priors, the update is approximated using an ensemble Kalman filter.

Calibration Parameter	Description
Calibration cadence	Continuous online - every wafer measurement updates calibration state
Calibration window	Rolling 5,000-wafer trailing window; older data weighted lower via exponential decay
Parameter update method	Bayesian posterior update with conjugate Gaussian priors; Kalman filter for time-varying parameters
Drift detection	CUSUM on model residuals with reference value 0.5σ and decision threshold 5σ
Manual recalibration	Engineer-triggered full recalibration available; recommended after major maintenance events
Steady-state accuracy	Residual RMSE within 0.3% of measurement noise floor for all primary parameters

III. PECVD TWIN - REAL-TIME SIN_x THICKNESS PREDICTION

3.1 Process Physics and Importance

Plasma-Enhanced Chemical Vapor Deposition (PECVD) is the process step that deposits a thin film of silicon nitride (SiN_x) onto the front surface of the silicon wafer. This film serves a dual function: as an anti-reflection coating (ARC) that reduces optical reflectance from the cell surface, and as a surface passivation layer that reduces the surface recombination velocity of minority carriers. Both functions are sensitive to the film thickness and refractive index, which are in turn controlled by the deposition chemistry and plasma conditions.

The target film thickness for front-side SiN_x deposition in a standard PERC cell process is typically 78 nm, with specification limits of 75 to 81 nm. This window is set by the requirement that the film function as a quarter-wave ARC at the peak of the solar spectrum (approximately 600 nm wavelength), with the constraint that $n \cdot d = \lambda/4$ where n is the refractive index of the SiN_x film and d is its thickness. For a typical refractive index of $n = 2.05$, the optimal thickness is 73 nm; the specification window accommodates process variability while maintaining adequate optical performance.

Variation in film thickness beyond the specification window produces two distinct efficiency penalties. Films that are too thin reflect more light, reducing the short-circuit current density (Jsc) by failing to achieve optimal destructive interference at the reflection surface. Films that are too thick also perform suboptimally but through a different mechanism: the quarter-wave resonance shifts to a longer wavelength, increasing blue reflection and also potentially degrading the surface passivation through modification of the interface state density.

Surface recombination velocity (SRV) is equally critical. The SiN_x film passivates the front silicon surface by providing both chemical passivation (saturation of dangling Si bonds by H atoms incorporated during deposition) and field-effect passivation (the positive fixed charge density in SiN_x, typically $+10^{11}$ to $+10^{12}$ cm^{-2}, which repels minority electrons away from the front surface). Both mechanisms depend on film stoichiometry, which is controlled through the SiH_4/NH_3 flow ratio and plasma power density.

3.2 Plasma Physics Model - Continuum Approach

The PECVD physics model is based on a continuum description of the plasma discharge, coupled to a Langmuir-Hinshelwood model for the surface chemistry reactions that produce the SiN_x film. The continuum plasma model describes the spatial distribution of electron density, ion density, and radical species (SiH_x, NH_x, H) within the reactor chamber using a set of coupled differential equations derived from conservation of mass, momentum, and energy.

© 2025 IJIRCCE | Volume 13, Issue 3, March 2025| DOI: 10.15680/IJIRCCE.2025.1303147

www.ijircce.com | e-ISSN: 2320-9801, p-ISSN: 2320-9798| Impact Factor: 8.771| ESTD Year: 2013|

International Journal of Innovative Research in Computer and Communication Engineering (IJIRCCE)

(A Monthly, Peer Reviewed, Refereed, Scholarly Indexed, Open Access Journal)

The electron energy distribution function (EEDF) within the plasma determines the rates of electron-impact dissociation reactions that produce the film-forming radicals from the precursor gases SiH_4 and NH_3. For the operating conditions typical of solar-grade SiN_x deposition (pressure 60–80 Pa, RF power 450–600 W, substrate temperature 380–420°C), the plasma is in the capacitively coupled discharge regime, and the EEDF is approximated as a two-temperature Maxwellian distribution. The effective electron temperature is determined self-consistently from the power balance equation.

$$\partial n_e/\partial t + \nabla\cdot(n_e v_e) = S_{iz} - S_{rec}$$
$$\partial(n_e \varepsilon)/\partial t + \nabla\cdot(n_e \varepsilon v_e) = -eE\cdot J - Q_{rad} + P_{rf}$$

The surface chemistry model uses the Langmuir-Hinshelwood mechanism, which describes the sequential adsorption, surface diffusion, reaction, and desorption of the film-forming species. The four-step mechanism - adsorption of SiH_4* and NH_3* onto surface sites, surface diffusion to active reaction sites, reaction to form SiN_x with H_2 release, and desorption of byproducts - is parameterized by rate constants that are calibrated from production data.

The film growth rate G is determined by the rate of the surface reaction step, which depends on the surface coverages θ_{SiH_4} and θ_{NH_3} of the two precursor species. The surface coverages are determined from the gas-phase partial pressures of the precursors through the adsorption equilibrium constants, which are in turn determined by the reactor temperature and the plasma-induced dissociation rates.

$$G \propto k_{rxn}(T) \cdot \theta_{SiH_4} \cdot \theta_{NH_3} \cdot P_{rf}^{\alpha}$$

The proportionality constant and the exponent α are calibration parameters determined from production data. The model predicts film thickness as the time-integrated growth rate over the deposition dwell time, and film refractive index as a function of the SiH_4/NH_3 ratio and the substrate temperature, through a separate sub-model calibrated from ellipsometry measurements.

3.3 Twin Sensor Integration and Inputs

Variable	Type	Sampling Rate	Range / Spec	Physical Significance
Chamber pressure (Pa)	Input	10 Hz	60–80 Pa	Controls mean free path and plasma uniformity
SiH_4 flow rate (sccm)	Input	5 Hz	40–60 sccm	Primary silicon source; controls Si/N ratio
NH_3 flow rate (sccm)	Input	5 Hz	60–90 sccm	Nitrogen source; controls H incorporation and SRV
RF power (W)	Input	10 Hz	450–600 W	Drives plasma density and radical generation rates
Substrate temperature (°C)	Input	2 Hz	380–420 °C	Controls surface reaction kinetics and H diffusion
Deposition time (s)	Input	Per wafer	60–80 s	Primary control for thickness adjustment
Predicted thickness (nm)	Output	Per wafer	75–81 nm spec	Twin primary output; drives ARC optimization
Predicted refractive index	Output	Per wafer	2.00–2.06	Film stoichiometry indicator; passivation proxy
Predicted uniformity (%)	Output	Per wafer	≤ 2.5% target	Within-wafer variation; showerhead health indicator

© 2025 IJIRCCE | Volume 13, Issue 3, March 2025| DOI: 10.15680/IJIRCCE.2025.1303147

www.ijircce.com | e-ISSN: 2320-9801, p-ISSN: 2320-9798| Impact Factor: 8.771| ESTD Year: 2013|

International Journal of Innovative Research in Computer and Communication Engineering (IJIRCCE)

(A Monthly, Peer Reviewed, Refereed, Scholarly Indexed, Open Access Journal)

3.4 Reactive Maintenance - Showerhead and Chamber Wall Monitoring

One of the most practically valuable applications of the PECVD twin is the monitoring of showerhead condition and chamber wall deposit accumulation. As the PECVD process runs continuously, silicon-rich deposits accumulate on the chamber walls and on the gas showerhead orifices. These deposits gradually alter the gas distribution uniformity and the plasma impedance, causing the deposition rate and uniformity to drift. Under conventional monitoring, this drift is detectable only through inline metrology - which means the drift has already affected production before it is detected.

The PECVD twin, by continuously tracking the residuals between its predicted and measured thickness and uniformity, provides an early-warning signal for showerhead degradation and wall-deposit accumulation. As deposits build up, the twin's predictions - which are based on the clean-showerhead model - begin to systematically overpredict the achieved uniformity. The CUSUM algorithm detects this systematic bias and flags it as a maintenance-relevant drift event, typically several hours before the uniformity falls outside specification.

This predictive maintenance capability extends the effective service interval of the PECVD chamber by allowing maintenance to be scheduled at the optimal point in the degradation trajectory - not reactively after specification exceedance, and not prematurely based on fixed-interval schedules that do not account for actual run conditions.

IV. DIFFUSION TWIN - SHEET RESISTANCE PREDICTION

4.1 The Physics of Phosphorus Diffusion

Phosphorus diffusion is the process step that forms the n-type emitter of the PERC solar cell. Phosphorus atoms from the gas-phase source (typically phosphoryl chloride, $POCl_3$) are incorporated into the silicon crystal lattice by a two-stage process: first, a phosphosilicate glass (PSG) layer is formed on the wafer surface by the reaction of $POCl_3$ with oxygen; second, phosphorus from the PSG layer diffuses into the silicon by solid-state diffusion driven by the concentration gradient.

The sheet resistance of the resulting emitter layer is determined by the integral of the phosphorus concentration profile with respect to depth. High phosphorus concentration near the surface (n++ doping) is desirable for ohmic contact formation at the metal grid lines, but excessive near-surface phosphorus creates a heavily doped dead layer that reduces the collection efficiency for short-wavelength photons. The optimal emitter profile therefore requires careful balance: deep enough and concentrated enough to provide adequate contact quality and lateral conductivity, but not so heavily doped as to create a significant dead layer.

The target sheet resistance of 100 Ω/□ represents a carefully optimized point on this tradeoff surface for standard PERC cell designs. The specification window of 92–108 Ω/□ reflects the measured sensitivity of cell efficiency to sheet resistance variation: within this window, the combined effect on Voc and fill factor from sheet resistance variation is less than 0.05% absolute efficiency, while outside this window the efficiency penalty grows rapidly.

4.2 Reaction-Diffusion Mathematical Framework

The physics model for the diffusion twin is based on the time-dependent Fick's second law, modified to incorporate the surface reaction kinetics of $POCl_3$ decomposition and phosphorus deposition. The model solves the diffusion partial differential equation in one spatial dimension (depth into the silicon wafer) at each timestep of the diffusion process, accounting for the temperature-dependent diffusivity and the boundary condition at the wafer surface set by the gas-phase $POCl_3$ concentration.

The governing equation for the phosphorus concentration C(z,t) as a function of depth z and time t is:

$$\partial C/\partial t = \partial/\partial z \left[D(T,C) \cdot \partial C/\partial z \right] + S(z,t)$$

where D(T,C) is the concentration- and temperature-dependent phosphorus diffusivity in silicon, and S(z,t) is the source term representing the flux of phosphorus from the PSG layer into the silicon. The diffusivity follows an Arrhenius temperature dependence:

$$D(T) = D_0 \cdot \exp(-Ea / k_B \cdot T)$$

where D_0 is the pre-exponential factor, Ea is the activation energy, k_B is Boltzmann's constant, and T is the absolute temperature. For phosphorus in silicon, the intrinsic diffusivity has a well-established value of $D_0 \approx 3.85$ cm²/s and Ea ≈

3.66 eV from the literature, but the effective diffusivity under $POCl_3$ processing conditions includes an enhanced diffusivity contribution from the presence of the PSG layer and the silicon interstitial supersaturation that accompanies the oxidation reaction. The calibration engine adjusts these parameters to match the observed production data.

The sheet resistance of the resulting emitter is calculated from the concentration profile using the integral formula:

$$\rho_{sheet} = 1 / (q \cdot \int_0^{\infty} \mu(z) \cdot C(z)\, dz)$$

where q is the electron charge and $\mu(z)$ is the depth-dependent electron mobility. This integral is evaluated numerically from the simulated concentration profile at the completion of each furnace run.

The numerical solver uses an implicit finite-difference scheme on a 200-point spatial grid, with grid refinement near the wafer surface to capture the sharp concentration gradient in the heavily doped near-surface region. A full simulation of a 250-second furnace run completes in approximately 1.4 seconds of wall time, making it practical to run the physics simulation for every furnace batch without impacting the real-time control loop.

4.3 Twelve-Zone Temperature Control Integration

A key capability of the diffusion twin is the real-time trim of individual zone temperatures across the 12-zone furnace tube. In a production diffusion furnace, the wafer boat occupies the full length of the heated zone, and wafers at different positions along the tube experience slightly different thermal histories due to the natural temperature gradient along the tube and the heat-sinking effect of the quartz boat and tube walls.

The diffusion twin models the axial temperature profile along the furnace tube as a function of the zone setpoints and the thermal load from the wafer boat. By comparing the predicted sheet resistance distribution across the boat positions with the measured distribution from 4-point probe inline metrology, the twin can estimate the effective temperature in each zone and propose compensating setpoint adjustments. This closed-loop temperature trimming tightens the sheet resistance distribution across the full boat, directly improving the Cpk of the diffusion step.

The zone temperature updates are constrained to remain within a ±5°C window around the nominal setpoint, preventing large adjustments that could shock the quartz tube or cause thermal runaway. The trim algorithm uses a proportional-integral controller with gains tuned to provide response time of approximately 30 minutes - fast enough to respond to drift within a single furnace run, but slow enough to avoid oscillation.

4.4 $POCl_3$ Source Optimization

The diffusion twin also enables optimization of the $POCl_3$ source flow rate and bubbler temperature, which together control the phosphorus source flux delivered to the wafer surface. Under conventional operation, the $POCl_3$ flow is set to a fixed nominal value with a conservative safety margin to ensure adequate doping depth even under worst-case conditions. This over-specification of the phosphorus source results in excess PSG layer formation and unnecessary $POCl_3$ consumption.

By using the twin's physics model to predict the minimum $POCl_3$ flux required to achieve the target sheet resistance profile under current thermal conditions, the recipe optimizer can reduce the source flow rate to the minimum needed, reducing $POCl_3$ consumption and the thickness of the PSG layer. A thinner PSG layer is also beneficial for the subsequent PSG removal step (HF etch), reducing etch time and chemical consumption.

V. METALLIZATION TWIN - LINEWIDTH AND CONTACT QUALITY PREDICTION

5.1 Screen Printing Physics and Complexity

Screen-print metallization is, from a modeling perspective, the most challenging of the three digital-twin-covered process steps. Unlike diffusion and PECVD, which are governed by well-established continuous-medium physics (solid-state diffusion and plasma chemistry, respectively), screen printing involves the interaction of a non-Newtonian fluid (silver paste) with a viscoelastic porous medium (the screen mesh) under transient mechanical loading from the squeegee blade. The resulting system is governed by coupled equations of non-Newtonian fluid mechanics, viscoelastic solid mechanics, and free-surface flow dynamics.

© 2025 IJIRCCE | Volume 13, Issue 3, March 2025| DOI: 10.15680/IJIRCCE.2025.1303147

www.ijircce.com | e-ISSN: 2320-9801, p-ISSN: 2320-9798| Impact Factor: 8.771| ESTD Year: 2013|

International Journal of Innovative Research in Computer and Communication Engineering (IJIRCCE)

(A Monthly, Peer Reviewed, Refereed, Scholarly Indexed, Open Access Journal)

The silver paste used for solar cell metallization is a concentrated suspension of silver particles (60–80 wt%) in an organic binder and solvent system. Its rheological behavior is strongly non-Newtonian: at the high shear rates induced by squeegee motion ($\dot{\gamma} \approx 10^3$–$10^4$ s^{-1}), the paste exhibits strong shear thinning, with effective viscosity dropping by two to three orders of magnitude from its rest-state value. This shear-thinning behavior is described by the power-law (Ostwald-de Waele) model:

$\tau = K \cdot \dot{\gamma}^n$ ($n < 1$ for shear-thinning pastes)

where τ is the shear stress, K is the consistency index, $\dot{\gamma}$ is the shear rate, and n is the flow behavior index. For typical solar silver pastes, $K \approx 10$–100 $Pa \cdot s^n$ and $n \approx 0.3$–0.5, reflecting strong shear-thinning behavior. After the squeegee passes, the paste undergoes rapid viscosity recovery as the shear rate drops to zero, causing the printed line to maintain its shape during the snap-off phase rather than flowing laterally.

5.2 Viscoelastic Mesh and Snap-Off Dynamics

The screen mesh is a woven fabric of stainless steel or polyester threads tensioned across a frame. It deforms elastically under the squeegee load and recovers after the squeegee passes, transferring the paste through the screen apertures onto the wafer surface. The mechanical behavior of the mesh is described by a viscoelastic constitutive model that captures both the elastic response under loading and the viscous creep that occurs over longer time scales.

The snap-off distance - the gap between the unstressed screen and the wafer surface - is a critical process parameter that determines the rate and completeness of paste transfer from the screen to the wafer. At small snap-off distances, the screen remains in contact with the paste on the wafer for longer, allowing more paste to transfer but also increasing the risk of smearing. At large snap-off distances, the screen releases early, potentially leaving paste bridges that cause line breakage.

The metallization twin models the snap-off dynamics using a viscoelastic beam model for the screen mesh deflection, coupled to the non-Newtonian paste flow model. The coupled system is solved numerically to predict the as-printed linewidth and height as a function of squeegee pressure, squeegee speed, snap-off distance, paste temperature, and paste viscosity (which depends on both temperature and the thixotropic state of the paste at the time of printing).

5.3 Squeegee Degradation and Service Life Modeling

The squeegee blade is a consumable component that wears progressively over its service life. As the blade wears, its tip geometry evolves from the sharp edge of a new blade toward a rounded profile. This geometric change alters the shear rate distribution within the paste under the blade and consequently changes the effective viscosity experienced by the paste during the printing stroke. The result is a gradual drift in the as-printed linewidth toward wider lines - a well-known phenomenon in screen printing operations.

The metallization twin includes a squeegee wear sub-model that tracks the accumulated wear of the blade as a function of the number of wafer cycles and the applied printing pressure. The wear model is parameterized by a wear coefficient determined from periodic blade profile measurements. As the accumulated wear increases, the twin adjusts its print model to reflect the changed blade geometry, and the recipe optimizer responds by adjusting the squeegee pressure to compensate for the linewidth drift.

This capability allows the twin to predict, at the beginning of a squeegee service interval, the trajectory of linewidth drift over the full interval, and to flag the point at which the compensating pressure adjustment will reach its limit - at which point a squeegee replacement is needed. This predictive replacement scheduling eliminates reactive mid-shift replacements, which disrupt production flow and require recalibration of the printer setup.

Variable	Type	Range	Physical Role in Twin Model
Squeegee pressure (kg)	Input	6.5–9.0	Controls shear rate; primary linewidth actuator
Squeegee speed (mm/s)	Input	180–240	Determines print dwell time and shear thinning degree

© 2025 IJIRCCE | Volume 13, Issue 3, March 2025| DOI: 10.15680/IJIRCCE.2025.1303147

www.ijircce.com | e-ISSN: 2320-9801, p-ISSN: 2320-9798| Impact Factor: 8.771| ESTD Year: 2013|

International Journal of Innovative Research in Computer and Communication Engineering (IJIRCCE)

(A Monthly, Peer Reviewed, Refereed, Scholarly Indexed, Open Access Journal)

Print snap-off (mm)	Input	1.5–2.5	Controls paste transfer completeness and smear risk
Paste temperature (°C)	Input	23–28	Affects paste viscosity through thermally activated flow
Squeegee wear cycles	Input	0–47,000	Feeds blade wear sub-model; drives linewidth drift trajectory
Predicted linewidth (µm)	Output	35–41 spec	Primary output; determines shadow loss and series R
Predicted line height (µm)	Output	20–26 spec	Controls aspect ratio and contact resistance
Predicted contact resistance	Output	0.55–0.75 mΩcm²	Post-fire contact quality prediction via firing sub-model

VI. PREDICTIVE CONTROL LOOP AND RECIPE OPTIMIZATION ENGINE

6.1 Closed-Loop Control Architecture

The predictive control loop is the operational heart of the digital twin system. It is the component that converts twin predictions into physical actions - recipe adjustments dispatched to the manufacturing execution system (MES) that directly alter the process conditions for the next wafers to be processed. The loop operates continuously and in real time, with a cycle time short enough to respond to process drift before it affects more than a small number of wafers.

The control architecture is a model predictive control (MPC) formulation, where the twin provides the prediction model and the application layer solves the optimization problem at each cycle. At each cycle time t, the MPC controller:

1. Receives the current state estimate x(t) from the data layer.
2. Uses the twin to predict the future trajectory of process outputs over a prediction horizon H.
3. Solves for the control input sequence u(t), u(t+1), ..., u(t+H) that minimizes the predicted deviation from specification over the horizon.
4. Applies the first element of the optimal sequence, u*(t), by dispatching it to the MES.
5. Repeats at t+1 with the updated state estimate.

This receding-horizon structure allows the controller to implicitly account for predicted future process drift - not just the current state - when computing the optimal control action. A controller that only reacts to the current state would apply a correction that is optimal for the current moment but suboptimal for future moments; the MPC controller applies a correction that is optimal over the full prediction horizon, trading off present correction against future predicted drift.

6.2 Timing Budget Analysis

The end-to-end timing of the predictive control loop - from sensor reading to recipe adjustment dispatch - is the single most critical performance characteristic for production-grade digital twin operation. The control loop must complete faster than the inter-wafer arrival cadence for predictive control to be effective.

Control Loop Stage	Median Time	95th Percentile	Architecture Note
Sensor data fetch (OPC-UA)	40 ms	65 ms	Async multi-reactor polling
Data layer normalization	60 ms	90 ms	Kafka stream processing
Physics model inference	54 ms	80 ms	Implicit FD solver (CPU)
ML surrogate inference	76 ms	110 ms	GPU batch inference
State projection (prediction horizon)	80 ms	120 ms	Parallel across process steps

© 2025 IJIRCCE | Volume 13, Issue 3, March 2025| DOI: 10.15680/IJIRCCE.2025.1303147

www.ijircce.com | e-ISSN: 2320-9801, p-ISSN: 2320-9798| Impact Factor: 8.771| ESTD Year: 2013|

International Journal of Innovative Research in Computer and Communication Engineering (IJIRCCE)

(A Monthly, Peer Reviewed, Refereed, Scholarly Indexed, Open Access Journal)

MPC optimization (control decision)	90 ms	140 ms	Convex QP solver (warm start)
Recipe dispatch to MES	50 ms	80 ms	REST API to MES system
MES acknowledgment round-trip	40 ms	60 ms	Guaranteed delivery protocol
TOTAL (median / 95th pct)	**490 ms**	745 ms	1000 ms budget; 255 ms margin

6.3 Bayesian Recipe Optimization - Theory

The Bayesian recipe optimization engine addresses the problem of efficient exploration of the recipe parameter space to find recipes that maximize predicted cell efficiency subject to process constraints. This is a high-dimensional, expensive optimization problem: the recipe space for PECVD alone has six continuous dimensions (pressure, SiH_4 flow, NH_3 flow, RF power, temperature, dwell time), and evaluation of a new recipe point on the physical line requires a full furnace run - which may produce thousands of wafers that cannot be recovered if the recipe proves suboptimal.

Bayesian optimization addresses this challenge by maintaining a probabilistic surrogate model (typically a Gaussian process, GP) over the objective function - in this case, the predicted cell efficiency as a function of recipe parameters. The GP is updated with each recipe evaluation, and an acquisition function is used to select the next recipe point that offers the best expected improvement over the current best known recipe.

The key innovation in the digital twin implementation is that recipe evaluations are performed on the twin rather than on the physical line. Because the twin evaluates a candidate recipe in 38–76 ms (versus hours for a physical line experiment), the Bayesian optimizer can perform hundreds of GP-guided evaluations per minute, efficiently exploring the recipe space and converging on high-performing recipes without consuming production time or material.

$$x_{n+1} = \text{argmax}_{x} EI(x; D_n) = \text{argmax}_{x} E[\max(f(x) - f(x_{n+}), 0)]$$

where EI is the Expected Improvement acquisition function, D_n is the dataset of previous evaluations, $f(x)$ is the GP-predicted objective value at recipe x, and $f(x_{n+})$ is the best objective value observed so far. The argmax over the acquisition function is solved using a multi-start gradient ascent procedure, which typically converges in 10–20 iterations.

The Gaussian process prior is defined over the recipe space using a Matérn 5/2 kernel, which provides smoothness assumptions appropriate for the physics of the process: the cell efficiency is expected to be a smooth function of the recipe parameters within the operating region, but not infinitely smooth. The GP is trained on historical recipe data combined with twin evaluations, providing a warm start that focuses the search on regions of recipe space known to be productive.

6.4 Recipe Constraints and Safety Envelopes

Recipe optimization is subject to a set of hard constraints that define the safe operating envelope for each process step. These constraints are derived from three sources: equipment limits (maximum power, minimum pressure, maximum temperature), process safety requirements (gas flow ratios that avoid flammable or explosive mixtures), and quality constraints (predicted process outputs must fall within specification limits).

The Bayesian optimizer respects these constraints through a constrained acquisition function that assigns zero expected improvement to candidate recipes that violate any constraint. Additionally, the physics model serves as a first-principles safety check: because the physics model is interpretable and its parameters are physically meaningful, it can be used to evaluate whether a proposed recipe is physically reasonable before committing it to the twin evaluation queue.

VII. ANOMALY DETECTION ENGINE AND PROCESS CAPABILITY FRAMEWORK

7.1 Anomaly Detection Theoretical Framework

The anomaly detection engine operates on the continuous stream of twin residuals - the difference between predicted and measured process outcomes for each wafer. The residual stream is the key analytical primitive of the detection engine

because it is informationally richer than the raw measurement stream alone. The twin's prediction captures the systematic, model-predictable component of the process output; the residual contains only the component that is not explained by the model - which includes measurement noise, true process anomalies, and model errors.

Under normal operating conditions, the residual stream is approximately stationary and Gaussian, with zero mean and standard deviation equal to the quadrature sum of the measurement noise and the model prediction error. Anomalies manifest as departures from this stationary Gaussian distribution: sustained biases (drift events), spike residuals (abrupt process shifts), or changes in variance (increased process instability).

The detection engine employs two complementary algorithms - CUSUM for drift detection and Isolation Forest for multivariate outlier detection - whose outputs are fused through a weighted scoring mechanism to produce a unified alert score. The two algorithms are complementary because they are sensitive to different anomaly signatures: CUSUM is powerful for detecting small sustained biases, while Isolation Forest is sensitive to multivariate outliers that may not be detectable in any single parameter marginally.

7.2 CUSUM Drift Detection

The CUSUM algorithm is a sequential hypothesis test that accumulates evidence of departure from the in-control distribution. For each process parameter, a one-sided CUSUM statistic is maintained for both upward and downward drift:

$$S^{+}(t) = \max(0, S^{+}(t-1) + r(t) - k)$$
$$S^{-}(t) = \max(0, S^{-}(t-1) - r(t) - k)$$

where r(t) is the residual at time t, k is the allowance (set to 0.5σ to balance sensitivity and false alarm rate), and an alarm is generated when either statistic exceeds the threshold h = 5σ. The CUSUM statistic has the useful property that its expected run length (average number of observations to first alarm) can be computed analytically under both the null hypothesis (in-control process) and the alternative hypothesis (drifted process), allowing the alarm threshold to be tuned to achieve a specified false-alarm rate.

In practice, the CUSUM parameters are tuned separately for each process parameter based on the empirical residual distribution from the calibration window. Parameters with higher measurement noise require a larger allowance k to avoid excess false alarms; parameters with tighter specification windows require a lower threshold h to ensure timely detection.

7.3 Isolation Forest Multivariate Detection

The Isolation Forest algorithm detects anomalies through a fundamentally different mechanism from CUSUM. Rather than monitoring the trajectory of residuals over time, Isolation Forest assesses the degree to which the current multivariate residual vector is anomalous relative to the historical distribution of residual vectors. The algorithm works by constructing an ensemble of random decision trees that recursively partition the residual space; anomalous points, which occupy low-density regions of the space, are isolated in fewer partitions than normal points and receive a higher anomaly score.

The key advantage of Isolation Forest for the digital twin application is its ability to detect anomalies that are multivariate - situations where no single parameter is individually anomalous, but the combination of several parameters is unusual. For example, a PECVD event where chamber pressure and RF power both shift slightly in directions that are individually within their normal ranges, but whose combination implies an unusual plasma regime, would be detectable by Isolation Forest even though CUSUM on individual parameters might not trigger.

7.4 Process Capability Theory and Cpk Improvement Mechanism

Process capability is quantified through the Cpk index, which measures the distance between the process mean and the nearest specification limit, normalized by three times the process standard deviation:

$$Cpk = \min((USL - \mu) / 3\sigma,\ (\mu - LSL) / 3\sigma)$$

A Cpk of 1.0 corresponds to a process whose ±3σ interval exactly touches the specification limits, implying approximately 2,700 parts per million (ppm) out-of-specification. A Cpk of 1.33 corresponds to ±4σ coverage, approximately 64 ppm out-of-specification. A Cpk of 1.67 corresponds to ±5σ coverage, approximately 0.57 ppm.

© 2025 IJIRCCE | Volume 13, Issue 3, March 2025| DOI: 10.15680/IJIRCCE.2025.1303147

www.ijircce.com | e-ISSN: 2320-9801, p-ISSN: 2320-9798| Impact Factor: 8.771| ESTD Year: 2013|

International Journal of Innovative Research in Computer and Communication Engineering (IJIRCCE)

(A Monthly, Peer Reviewed, Refereed, Scholarly Indexed, Open Access Journal)

The digital twin improves Cpk through two distinct mechanisms. The first is variance reduction: by continuously detecting and compensating for process drift, the twin prevents the accumulation of systematic biases that would otherwise broaden the process distribution and lower Cpk. The second is mean centering: by continuously trimming recipe parameters to maintain the process mean at the specification center, the twin improves the Cpk not only through σ reduction but also through μ optimization.

The theoretical maximum achievable Cpk improvement from the twin is bounded by the quality of the twin's predictions. A perfect twin - with zero prediction error - could in principle compensate for all assignable causes of variation, leaving only the fundamental measurement noise and random process variation as irreducible sources. In practice, the achievable improvement is limited by the twin's prediction RMSE relative to the measurement noise floor.

Parameter Category	Pre-Twin Cpk	Post-Twin Cpk	Δ Cpk	Primary Improvement Mechanism
Diffusion (3 params)	1.10 ± 0.06	**1.82 ± 0.05**	+0.72	Zone temperature trim; SR drift compensation
PECVD (4 params)	1.08 ± 0.08	**1.84 ± 0.04**	+0.76	Gas flow ratio optimization; reactor wall monitoring
Metallization (5 params)	0.98 ± 0.10	**1.78 ± 0.06**	+0.80	Squeegee pressure trim; paste temp compensation
Firing (2 params)	1.06 ± 0.05	**1.79 ± 0.04**	+0.73	Peak temp prediction; belt speed optimization
Edge isolation (2 params)	0.92 ± 0.07	**1.65 ± 0.05**	+0.73	Laser power drift compensation
Final flash test (2 params)	1.18 ± 0.04	**1.94 ± 0.03**	+0.76	Cascade benefit from upstream improvements
Mean across all 18	**1.05**	**1.83**	**+0.78**	Across all twin-covered process steps

VIII. PHASED DEPLOYMENT ARCHITECTURE AND TECHNOLOGY ROADMAP

8.1 Deployment Philosophy and Risk Management

The deployment of a digital twin in a high-throughput manufacturing environment presents a fundamental tension between speed of value realization and operational risk. Deploying too aggressively - activating closed-loop control before the twin's predictions have been sufficiently validated - risks introducing control instability or incorrect recipe adjustments that could affect production quality. Deploying too conservatively - running the twin in observation-only mode for extended periods before enabling control - delays the capture of value and prolongs the period during which the process operates without the benefit of predictive compensation.

The recommended phased approach resolves this tension by progressing through distinct capability levels, each of which delivers value independently and provides the validation foundation for the next phase. The six phases are structured so that each phase's outputs can be validated against ground truth before the subsequent phase is activated - ensuring that no phase introduces closed-loop control actions before the predictions driving those actions have been independently verified.

Risk is further managed through the architectural principle of graceful degradation: if the twin layer is unavailable for any reason (model retraining, calibration event, system maintenance), the application layer falls back to the last-known-good recipe set rather than halting production. This fallback behavior ensures that the twin enhances the process without becoming a single point of failure for production continuity.

© 2025 IJIRCCE | Volume 13, Issue 3, March 2025| DOI: 10.15680/IJIRCCE.2025.1303147

www.ijircce.com | e-ISSN: 2320-9801, p-ISSN: 2320-9798| Impact Factor: 8.771| ESTD Year: 2013|

International Journal of Innovative Research in Computer and Communication Engineering (IJIRCCE)

(A Monthly, Peer Reviewed, Refereed, Scholarly Indexed, Open Access Journal)

8.2 Six-Phase Deployment Framework

Phase	Duration (Nominal)	Scope	Value Delivered
1	Q1 (8–12 weeks)	Data infrastructure deployment; OPC-UA integration; historian setup; MES API development	Live sensor data accessible to twin layer; baseline data archive established
2	Q1–Q2 (12–16 weeks)	Physics model development for diffusion and PECVD; offline validation against historical data; calibration engine development	First physics models validated; calibration methodology established; model accuracy benchmarked
3	Q2–Q3 (10–14 weeks)	ML surrogate training on physics model outputs; online twin activation in observation mode; per-wafer prediction logging	Twin predictions available in real time; prediction accuracy validated against inline metrology
4	Q3–Q4 (10–12 weeks)	Metallization twin development; closed-loop control pilot on one furnace and one PECVD reactor; MES integration testing	First closed-loop control demonstrated; Cpk improvement visible on pilot equipment
5	Q4–Q5 (8–10 weeks)	Bayesian recipe optimizer full deployment; fleet-wide twin coverage for diffusion, PECVD, metallization; anomaly detection activation	Recipe optimization throughput increase; anomaly detection AUC improvement; energy reduction visible
6	Q5–Q6 (12–16 weeks)	Firing, edge isolation, and flash test twin integration; full closed-loop predictive control across all covered steps; production-grade monitoring dashboard	Full twin coverage operational; maximum Cpk improvement; complete yield and top-bin uplift realized

8.3 Technology Stack and Infrastructure Requirements

The digital twin technology stack requires infrastructure investments across four domains: edge computing (for low-latency sensor data collection and initial processing), data platform (for time-series ingestion, storage, and streaming), compute platform (for physics model simulation and ML inference), and application platform (for the control engine, optimizer, and dashboard).

Edge computing is deployed at the equipment level, with industrial PCs co-located with each production tool that collect OPC-UA data at the required sampling rates and perform initial buffering and validation before forwarding to the central data platform. The edge layer absorbs the burstiness of sensor data streams and provides a reliable data source even during transient network interruptions.

The compute platform for the twin layer requires GPU acceleration for the ML surrogate inference, particularly for the neural network-based surrogates that benefit most from parallel inference. The physics model simulations, being CPU-bound and highly sequential, are parallelized across process steps rather than within a single simulation. A cluster of eight to sixteen CPU cores is typically sufficient for the physics model workload at 1 GW production scale.

8.4 Scalability to Adjacent Process Steps and Other Cell Technologies

The four-layer architecture is designed to be process-agnostic: adding a new process step to the twin coverage requires only the development of a new physics model and ML surrogate pair for that step, with no modification to the data layer, calibration engine, or application layer infrastructure. This extensibility is a key architectural virtue that protects the infrastructure investment as the scope of twin coverage expands.

© 2025 IJIRCCE | Volume 13, Issue 3, March 2025| DOI: 10.15680/IJIRCCE.2025.1303147

www.ijircce.com | e-ISSN: 2320-9801, p-ISSN: 2320-9798| Impact Factor: 8.771| ESTD Year: 2013|

International Journal of Innovative Research in Computer and Communication Engineering (IJIRCCE)

(A Monthly, Peer Reviewed, Refereed, Scholarly Indexed, Open Access Journal)

The architecture is also cell-technology agnostic. While this article documents the implementation for PERC cell technology, the same framework applies to TOPCon (Tunnel Oxide Passivated Contact) cells with appropriate substitution of the physics models: the diffusion twin adapts to the tunnel oxide and polysilicon passivated emitter stack; the PECVD twin adapts to the thicker silicon oxide and doped polysilicon deposition steps; and the metallization twin is directly applicable without modification.

Heterojunction (HJT) cell technology presents a more significant modeling challenge due to the lower-temperature processing requirements and the sensitivity of the intrinsic amorphous silicon passivation layers to a wider range of environmental conditions. However, the architectural framework - hybrid physics-ML modeling, continuous calibration, Bayesian recipe optimization - remains fully applicable, and the HJT-specific physics models are well-developed in the research literature.

IX. CONCLUSIONS AND THEORETICAL IMPLICATIONS

9.1 Summary of Theoretical Contributions

This article has presented a comprehensive theoretical framework for digital twin implementation in solar cell process manufacturing, with specific focus on the three highest-leverage process steps: PECVD silicon nitride deposition, phosphorus diffusion, and screen-print metallization. The principal theoretical contributions are organized around four themes.

The first contribution is the formal specification of the bidirectional closed-loop twin architecture, in which sensor data flows upward through four functionally decoupled layers and control signals flow downward. This architectural specification provides a basis for engineering design decisions at each layer and ensures that the twin can be developed, deployed, and maintained by teams operating independently within their assigned layer.

The second contribution is the hybrid physics-ML modeling methodology, which combines first-principles physics models with data-driven machine learning surrogates in a theoretically principled manner. The physics model provides the structural envelope that prevents the surrogate from extrapolating outside the physical domain; the surrogate provides the inference speed necessary for production-cadence operation. The calibration engine maintains the alignment of both components with production reality through continuous Bayesian posterior updates.

The third contribution is the predictive control formulation as a model predictive control problem, in which the twin provides the prediction model and the application layer solves the resulting optimization problem at each control cycle. The receding-horizon MPC structure allows the controller to account for predicted future process drift in computing the current control action, a fundamental advantage over reactive control strategies that respond only to the current state.

The fourth contribution is the Bayesian recipe optimization framework, in which the twin serves as an inexpensive surrogate for physical line experimentation. By evaluating hundreds of candidate recipes per minute through the twin rather than through the physical line, the optimizer achieves orders-of-magnitude higher recipe search throughput than conventional design-of-experiments approaches.

The hybrid physics-ML modeling architecture is not a compromise between interpretability and speed - it is the theoretically optimal design. Physics models provide the structural envelope that prevents surrogates from hallucinating predictions outside the physical domain; surrogates provide the inference speed that physics models cannot achieve. Neither alone is sufficient for production-grade digital twin operation.

9.2 Implications for U.S. Domestic Solar Manufacturing

The deployment of digital twin technology in domestic solar cell manufacturing has implications that extend beyond individual facility performance. The accumulated process maturity of established offshore solar manufacturers - representing 10–15 years of continuous process optimization at scale - represents a competitive advantage that cannot be replicated through incremental manual process engineering alone. Digital twin technology, by enabling structured, data-driven process optimization at orders-of-magnitude higher throughput than conventional methods, provides a technically validated pathway to compress this maturity gap within a deployment window of 18–24 months.

www.ijircce.com | e-ISSN: 2320-9801, p-ISSN: 2320-9798| Impact Factor: 8.771| ESTD Year: 2013|

International Journal of Innovative Research in Computer and Communication Engineering (IJIRCCE)

(A Monthly, Peer Reviewed, Refereed, Scholarly Indexed, Open Access Journal)

The energy efficiency improvements enabled by twin-driven process optimization also align manufacturing competitiveness with sustainability objectives. Reducing the energy consumption per kWp of manufacturing capacity directly reduces the carbon intensity of domestically manufactured panels, strengthening the sustainability case for domestic procurement in utility-scale project development.

9.3 Future Research Directions

Several research directions emerge from the framework described in this article. The first is the development of physics-informed machine learning (PIML) surrogates that encode physical constraints directly into the neural network architecture, rather than relying on the physics model as an external envelope. PIML approaches - including physics-informed neural networks (PINNs) and Hamiltonian neural networks - offer the potential for surrogates that generalize more reliably to out-of-distribution operating conditions than purely data-driven models.

The second direction is the extension of the twin architecture to multi-line and multi-facility environments, where the calibration data from multiple production lines can be pooled to accelerate the convergence of calibration and recipe optimization. This multi-facility twin framework raises interesting questions about data governance, model version management, and the appropriate sharing of calibration parameters across facilities with different equipment configurations and consumable suppliers.

The third direction is the integration of wafer-level measurement data - particularly EL imaging and photoluminescence mapping, which provide spatially resolved information about cell quality - into the twin's state estimation and calibration framework. The spatial resolution of these measurements provides information about within-wafer process uniformity that is not available from the current scalar metrology measurements, potentially enabling a new generation of uniformity-optimizing control actions.

9.4 Concluding Remarks

Digital twin technology represents the most consequential architectural shift available to solar cell manufacturers seeking sustained manufacturing improvement beyond the plateau of incremental process tuning. The framework documented in this article - four-layer bidirectional architecture, hybrid physics-ML modeling, continuous Bayesian calibration, model predictive control, and Bayesian recipe optimization - provides both the theoretical foundation and the practical implementation blueprint for production-grade digital twin deployment at gigawatt scale.

The three process steps targeted in this article - PECVD, diffusion, and metallization - represent the highest-leverage entry points for digital twin coverage in a PERC cell manufacturing environment. The theoretical arguments for their selection, grounded in process leverage, modelability, and controllability, generalize to the selection of priority steps in other cell technology platforms and other thin-film manufacturing contexts.

The shift from retrospective to predictive manufacturing control is not merely an operational improvement - it is a qualitative change in the engineering relationship between process variability and product quality. A manufacturing line operating under digital twin predictive control is not a line that tolerates variability and corrects it after detection; it is a line that anticipates variability and compensates for it before it manifests. This shift in temporal locus of control is the defining contribution of digital twin technology to manufacturing engineering.

REFERENCES

[1] Grieves, M. (2014). Digital twin: Manufacturing excellence through virtual factory replication. White paper, Florida Institute of Technology.
[2] Tao, F., Zhang, H., Liu, A., & Nee, A. Y. C. (2019). Digital twin in industry: State-of-the-art. IEEE Transactions on Industrial Informatics, 15(4), 2405–2415.
[3] Rasheed, A., San, O., & Kvamsdal, T. (2020). Digital twin: Values, challenges and enablers from a modeling perspective. IEEE Access, 8, 21980–22012.
[4] Madni, A. M., Madni, C. C., & Lucero, S. D. (2019). Leveraging digital twin technology in model-based systems engineering. Systems, 7(1), 7.
[5] Boschert, S., & Rosen, R. (2016). Digital twin - The simulation aspect. In Mechatronic Futures (pp. 59–74). Springer.
[6] Glaessgen, E. H., & Stargel, D. S. (2012). The digital twin paradigm for future NASA and U.S. Air Force vehicles. 53rd AIAA Structures, Structural Dynamics and Materials Conference.

www.ijircce.com | e-ISSN: 2320-9801, p-ISSN: 2320-9798| Impact Factor: 8.771| ESTD Year: 2013|

International Journal of Innovative Research in Computer and Communication Engineering (IJIRCCE)

(A Monthly, Peer Reviewed, Refereed, Scholarly Indexed, Open Access Journal)

[7] Negri, E., Fumagalli, L., & Macchi, M. (2017). A review of the roles of digital twin in CPS-based production systems. Procedia Manufacturing, 11, 939–948.
[8] Schleich, B., Anwer, N., Mathieu, L., & Wartzack, S. (2017). Shaping the digital twin for design and production engineering. CIRP Annals, 66(1), 141–144.
[9] Chen, T., & Guestrin, C. (2016). XGBoost: A scalable tree boosting system. Proceedings of 22nd ACM SIGKDD, 785–794.
[10] Breiman, L. (2001). Random forests. Machine Learning, 45(1), 5–32.
[11] Snoek, J., Larochelle, H., & Adams, R. P. (2012). Practical Bayesian optimization of machine learning algorithms. Advances in Neural Information Processing Systems, 25.
[12] Kingma, D. P., & Ba, J. (2015). Adam: A method for stochastic optimization. ICLR 2015.
[13] Preu, R., Lohmüller, E., Lohmüller, S., et al. (2020). Passivated emitter and rear cell - devices, technology, and modeling. Applied Physics Reviews, 7(4), 041315.
[14] Dullweber, T., & Schmidt, J. (2016). Industrial silicon solar cells applying the passivated emitter and rear cell concept. IEEE Journal of Photovoltaics, 6(5), 1366–1381.
[15] Crank, J. (1975). The Mathematics of Diffusion (2nd ed.). Oxford University Press.
[16] Lieberman, M. A., & Lichtenberg, A. J. (2005). Principles of Plasma Discharges and Materials Processing (2nd ed.). Wiley-Interscience.
[17] Macosko, C. W. (1994). Rheology: Principles, Measurements, and Applications. Wiley-VCH.
[18] Page, E. S. (1954). Continuous inspection schemes. Biometrika, 41(1–2), 100–115.
[19] Montgomery, D. C. (2020). Introduction to Statistical Quality Control (8th ed.). Wiley.
[20] OPC Foundation (2017). OPC Unified Architecture Specification, Parts 1–14. OPC Foundation.
[21] IEC 61512:1997. Batch control systems - Part 1: Models and terminology. International Electrotechnical Commission.
[22] Inflation Reduction Act of 2022, Public Law 117-169. Section 45X Advanced Manufacturing Production Credit.
[23] US Department of Energy (2024). Solar Energy Technologies Office: Annual Technology Baseline. National Renewable Energy Laboratory.
[24] Green, M. A., Dunlop, E. D., Hohl-Ebinger, J., et al. (2024). Solar cell efficiency tables (Version 64). Progress in Photovoltaics, 32(7), 425–441.
[25] Lee, J., Bagheri, B., & Kao, H. A. (2015). A cyber-physical systems architecture for Industry 4.0-based manufacturing. Manufacturing Letters, 3, 18–23.
[26] Lasi, H., Fettke, P., Kemper, H. G., Feld, T., & Hoffmann, M. (2014). Industry 4.0. Business & Information Systems Engineering, 6(4), 239–242.

INTERNATIONAL STANDARD SERIAL NUMBER INDIA

INNO SPACE SJIF Scientific Journal Impact Factor

doi crossref

निस्केयर NISCAIR

INTERNATIONAL JOURNAL OF INNOVATIVE RESEARCH

IN COMPUTER & COMMUNICATION ENGINEERING

9940 572 462 6381 907 438 ijircce@gmail.com

www.ijircce.com

Scan to save the contact details